Joint Estimation of Vertical Total Electron Content (VTEC) and Satellite Differential Code Biases (SDCBs) Using Low-cost Receivers

Baocheng Zhang[1*], Peter J.G. Teunissen[2, 3*], Yunbin Yuan[1], Hongxing Zhang[1], Min Li[1]

E-mails: b.zhang@whigg.ac.cn

p.teunissen@curtin.edu.au

Tel: 86-27-6888 1072

Fax: 86-27-8678 3841

1. State Key Laboratory of Geodesy and Earth's Dynamics, Institute of Geodesy and Geophysics, Chinese Academy of Sciences, Wuhan, China
2. Global Navigation Satellite System (GNSS) Research Centre, Curtin University, Perth, Australia
3. Geoscience and Remote Sensing, Delft University of Technology, Delft, The Netherlands

Abstract

Vertical Total Electron Content (VTEC) parameters estimated using Global Navigation Satellite System (GNSS) data are of great interest for ionosphere sensing. Satellite Differential Code Biases (SDCBs) account for one source of error which, if left uncorrected, can deteriorate performance of positioning, timing and other applications. The customary approach to estimate VTEC along with SDCBs from dual-frequency GNSS data, hereinafter referred to as DF approach, consists of two sequential steps. The first step seeks to retrieve ionospheric observables through the Carrier-to-Code Leveling (CCL) technique. This observable, related to the Slant Total Electron Content (STEC) along the satellite-receiver line-of-sight, is biased also by the SDCBs and the Receiver Differential Code Biases (RDCBs). By means of thin-layer ionospheric model, in the second step one is able to isolate the VTEC, the SDCBs and the RDCBs from the ionospheric observables. In this work, we present a

single-frequency (SF) approach, enabling the joint estimation of VTEC and SDCBs using low-cost receivers; this approach is also based on two steps and it differs from the DF approach only in the first step, where we turn to the Precise Point Positioning (PPP) technique to retrieve from the single-frequency GNSS data the ionospheric observables, interpreted as the combination of the STEC, the SDCBs and the biased receiver clocks at the pivot epoch. Our numerical analyses clarify how SF approach performs when being applied to GPS L1 data collected by a single receiver under both calm and disturbed ionospheric conditions. The daily time series of zenith VTEC estimates has an accuracy ranging from a few tenths of a TEC unit (TECU) to approximately 2 TECU. For 73 to 96 percent of GPS satellites in view, the daily estimates of SDCBs do not deviate, in absolute value, more than 1 nanosecond from their ground-truth values published by the Centre for Orbit Determination in Europe (CODE).

Keywords

Global Navigation Satellite System (GNSS); Vertical Total Electron Content (VTEC); Satellite Differential Code Biases (SDCBs); Carrier-to-Code Leveling (CCL); Precise Point Positioning (PPP); Thin-layer ionospheric model

1. Introduction

Global Navigation Satellite System (GNSS) data are a valuable source of information for sensing the Earth's ionosphere (Hernández-Pajares et al. 1999; Komjathy et al. 2005; Li et al. 2015; Liu and Gao 2004; Mannucci et al. 1993). Although the ionospheric parameters that one can estimate from GNSS data are various (Dyrud et al. 2008; Lognonné et al. 2006; Yao et al. 2013), the Vertical Total Electron Content (VTEC) is generally the most widely used (Brunini and Azpilicueta 2010; Brunini and Azpilicueta 2009); its empirical importance lies in contributing useful understanding to the physics behind different space weather phenomena (Gulyaeva et al. 2014; Komjathy et al. 2012), in providing valuable insights into the possible causes of natural and man-made hazardous events (Artru et al. 2005; Dautermann et al. 2007;

Park et al. 2011), and in delivering corrections to the ionospheric effects on signals transmitted by the other space geodetic techniques than by the GNSS (Dettmering et al. 2014; Sardon et al. 1994b). On the other hand, the Satellite Differential Code Biases (SDCBs), defined as the deviations of the satellite code instrumental delays on one frequency from their counterparts on another frequency (Sardon et al. 1994a), account for one major source of error in Positioning, Navigation and Timing (PNT) applications that employ undifferenced GNSS code and phase data (Montenbruck et al. 2014; Wang et al. 2016). This justifies the need for first estimating the SDCBs and then delivering the estimates to interested PNT users.

Usually, the approach for jointly estimating the VTEC and the SDCBs involves the use of GNSS data on two frequencies, and thus requires the participation of one or more geodetic-grade receivers. Hereinafter, we refer to this approach as dual-frequency (DF) approach, which, in principle, is comprised of two sequential steps (Banville et al. 2014; Ciraolo et al. 2007; Stephens et al. 2011). In the first step, one aligns the precise but ambiguous phase to the noisy but absolute code observables on an arc-by-arc basis, thereby yielding the ionospheric observables that are a combination of the Slant Total Electron Content (STEC), the SDCBs and the Receiver Differential Code Biases (RDCBs). This procedure is termed as Carrier-to-Code Leveling (CCL) technique (Brunini and Azpilicueta 2010; Brunini et al. 2008). The second step concerns the application of thin-layer ionospheric model to those ionospheric observables (Brunini et al. 2011), from which the VTEC, the SDCB as well as the RDCB estimates arise.

Although not everyone agrees that the DF approach may be by far the state-of-the-art, it continues to serve the needs of the ionospheric community. Here we briefly revisit two typical uses of this approach. The first use is to produce the snapshots of the global VTEC in the form of Global Ionosphere Maps (GIMs) on a regular basis, a routine task that the International GNSS Service (IGS) generally carries out (Feltens 2003; Hernández-Pajares et al. 2009; Mannucci et al. 1998). The second use, which we shall consider in our analysis, is to generate local VTEC using GNSS data from a single receiver. This use is in particular beneficial for monitoring

the spatial and temporal evolution of the ionosphere over a given location (Choi et al. 2012; Sezen et al. 2013). At the same time, the attractiveness of DF approach lies also in its ability to provide SDCB estimates as by-products.

Note, interestingly, that, there is a vast body of literature on a single-frequency (SF) approach, estimating VTEC from the Code-Minus-Phase (CMP) observables (Cohen et al. 1992; Schüler and Oladipo 2013; Schüler and Oladipo 2014; Xia 1992). One prominent advantage over the DF approach is that the SF approach is more cost-effective because it relies upon mass-market (instead of geodetic-grade) receivers. However, the inability of the SF approach to estimate SDCBs (along with VTEC) remains a bottleneck problem. This comes as no surprise, since CMP observables do not encompass the SDCBs.

In this work, we propose a novel SF approach, enabling the joint estimation of VTEC and SDCBs from the original GNSS code and phase observables. Our approach consists also of two steps and it differs from the DF approach only in the first step, where we correct the original GNSS data with the precise satellite orbit and clock products delivered by the IGS so as to construct the observed-minus-computed observations, and then process them into the ionospheric observables through the Precise Point Positioning (PPP) technique (Zumberge et al. 1997). As we shall detail in the next section, these observables contain the STEC, the SDCBs and the biased receiver clocks at the first (pivot) epoch, and one can thus estimate from them the VTEC and the SDCBs with the thin-layer ionospheric model. This is the main contribution of this work.

The organization of this work proceeds as follows. Section 2 reviews in brief the basic principles and technological aspects of the CCL technique, and then describes in detail how to deal with the rank deficiencies underlying the original code and phase observation equations, a key issue to be addressed for the development of PPP technique. We close this section with an introduction to the main formulae of the thin-layer ionospheric model. Section 3 presents the experimental results from applying our SF and the DF approaches to GPS data collected by receivers of different types and manufactures under all possible ionospheric conditions, in seeking to

clarify the overall performance of our SF approach in estimating the VTEC and the SDCBs using a single GPS receiver. We conclude in Section 4.

2. Methodology

This section starts with a review of CCL technique, proceeds to PPP technique, and ends with a presentation of thin-layer ionospheric model.

Carrier-to-Code Leveling (CCL)

For completeness let us first present the CCL technique, which constitutes the first step of the DF approach. The point of departure is the system of linear observation equations, which reads (Leick et al. 2015),

$$\begin{aligned} p_{r,j}^{s}(i) &= \rho_{r}^{s}(i) + \mu_{j} t_{r}^{s}(i) - d_{,j}^{s} + d_{r,j} \\ \phi_{r,j}^{s}(i) &= \rho_{r}^{s}(i) - \mu_{j} t_{r}^{s}(i) + a_{r,j}^{s} \end{aligned} \tag{1}$$

with r, s, j and i the receiver, satellite, frequency and epoch indices, and where $p_{r,j}^{s}(i)$ and $\phi_{r,j}^{s}(i)$ denote, respectively, the code and the phase observables. Here we consider a measurement scenario that one GNSS receiver tracks dual-frequency code and phase data from a total of m satellites over t epochs, thereby implying $r=1$, $s=1,\cdots,m$, $j=1,2$ and $i=1,\cdots,t$. The parameters include, $\rho_{r}^{s}(i)$ the combination of all frequency-independent effects, $t_{r}^{s}(i)$ the STEC experienced on the first frequency with coefficients $\mu_{j}=\lambda_{j}^{2}/\lambda_{1}^{2}$ and λ_{j} the wavelength, $d_{,j}^{s}$ the satellite code instrumental delays and $d_{r,j}$ the receiver counterparts, $a_{r,j}^{s}$ the real-valued ambiguities absorbing the phase instrumental delays. All parameters are expressed in units of range, except $t_{r}^{s}(i)$, to which a unit conversion from meters to Total Electron Content Units (TECU) is applied after the estimation process. The sensitivity of the ionospheric range delay to STEC for the GPS L1 signal is 0.162 meters per TECU. The parameters assigned with epoch index i are assumed time-varying, whereas the remainders are assumed time-constant.

There are three interrelated tasks that one needs to undertake.

The first task is to construct geometry-free code and phase observation equations,

taking the following forms,

$$\begin{aligned} p^s_{r,gf}(i) &= \mu_{gf}\iota^s_r(i) - d^s_{gf} + d_{r,gf} \\ \phi^s_{r,gf}(i) &= -\mu_{gf}\iota^s_r(i) + a^s_{r,gf} \end{aligned} \tag{2}$$

with $(\cdot)_{gf} = (\cdot)_{,2} - (\cdot)_{,1}$ the operator creating a geometry-free variable. Note that, $d^s_{gf} = d^s_{,2} - d^s_{,1}$ and $d_{r,gf} = d_{r,2} - d_{r,1}$ denote, respectively, the SDCBs and the RDCBs.

In the second task, we compute, on an arc-by-arc basis, an offset between $p^s_{r,gf}(i)$ and $\phi^s_{r,gf}(i)$, which, denoted here using $\tilde{a}^s_{r,gf}$, amounts to the weighted average of $\left[p^s_{r,gf}(i) + \phi^s_{r,gf}(i)\right]$ over t epochs ($i = 1, \cdots, t$). Hence, it follows that the interpretation of $\tilde{a}^s_{r,gf}$ reads,

$$\tilde{a}^s_{r,gf} = a^s_{r,gf} - d^s_{gf} + d_{r,gf} \tag{3}$$

where $\tilde{a}^s_{r,gf}$ is known as leveling bias.

The third task applies $\tilde{a}^s_{r,gf}$ to $\phi^s_{r,gf}(i)$, so as to yield the ionospheric observables $\tilde{\iota}^s_r(i)$,

$$\begin{aligned} \tilde{\iota}^s_r(i) &= -\frac{1}{\mu_{gf}}\left[\phi^s_{r,gf}(i) - \tilde{a}^s_{r,gf}\right] \\ &= \iota^s_r(i) - \frac{1}{\mu_{gf}}\left(d^s_{gf} - d_{r,gf}\right) \end{aligned} \tag{4}$$

where we see that, this ionospheric observable is a linear combination of the original STEC $\iota^s_r(i)$, one SDCB d^s_{gf} and one RDCB $d_{r,gf}$.

Precise Point Positioning (PPP)

We base our derivation on the single-frequency ($j = 1$) variant of Equation (1), which reads,

$$\begin{aligned} p^s_{r,1}(i) &= \rho^s_r(i) + \iota^s_r(i) - d^s_{,1} + d_{r,1} \\ \phi^s_{r,1}(i) &= \rho^s_r(i) - \iota^s_r(i) + a^s_{r,1} \end{aligned} \tag{5}$$

where we consider the fact that $\mu_1 = 1$.

We first of all re-write $\rho^s_r(i)$ in the form,

$$\rho^s_r(i) = g^s_r(i) + \tau^s_r(i) - dt^s(i) + dt_r(i) \tag{6}$$

with $g^s_r(i)$ the geometric ranges, $\tau^s_r(i)$ the slant tropospheric delays, $dt^s(i)$

the satellite clocks and $dt_r(i)$ the receiver clocks.

Next we take advantage of precise satellite orbit and clock products externally provided, from which a-priori known satellite positions $x^s(i)$ and satellite clocks $\widehat{dt}^s(i)$ arise. Note, importantly, that, $\widehat{dt}^s(i)$ are biased and read (Kouba and Héroux 2001),

$$\widehat{dt}^s(i) = dt^s(i) + d_{if}^s \tag{7}$$

with $d_{if}^s = \frac{1}{\mu_{gf}}\left(\mu_2 d_{,1}^s - d_{,2}^s\right)$ the ionosphere-free satellite code instrumental delays.

Furthermore, let us assume that the receiver positions $x_r(i)$ are a-priori known; this is a sensible assumption, since one inclines to deploy GNSS receivers at known locations in the area of interest when sensing the ionosphere. Additionally, we make use of an empirical model to compute approximate values for $\tau_r^s(i)$, denoted using $\tau_r^{s,0}(i)$.

Incorporating these considerations into Equation (5) one obtains

$$\begin{aligned}\widehat{p}_{r,1}^s(i) &= c_r^s(i)\cdot\widehat{\tau}_r(i) + d_{if}^s + dt_r(i) + \iota_r^s(i) - d_{,1}^s + d_{r,1} \\ \widehat{\phi}_{r,1}^s(i) &= c_r^s(i)\cdot\widehat{\tau}_r(i) + d_{if}^s + dt_r(i) - \iota_r^s(i) + a_{r,1}^s\end{aligned} \tag{8}$$

where $\widehat{p}_{r,1}^s(i)$ denotes the corrected code observables, resulting from applying the a-priori known geometric ranges $g_r^s(i)$, the a-priori known satellite clocks $\widehat{dt}^s(i)$ and the approximate slant tropospheric delays $\tau_r^{s,0}(i)$ to the original code observable $p_{r,1}^s(i)$; likewise, $\widehat{\phi}_{r,1}^s(i)$ denotes the corrected phase observables. Notably, here we decompose $\rho_r^s(i)$ into three types of parameters, including the zenith tropospheric delays (ZTDs) $\widehat{\tau}_r(i)$ with mapping functions given as $c_r^s(i)$, the ionosphere-free satellite code instrumental delays d_{if}^s and the receiver clocks $dt_r(i)$.

Equation (8) represents a rank-deficient system, with which one cannot estimate the parameters uniquely. We tend to eliminate the rank deficiency in this equation, of size $2(m+1)$, by means of re-parameterization.

We focus first on the code observation equations. The idea is to lump the $\iota_r^s(i)$,

the d_{if}^{s} and the $d_{,1}^{s}$, thereby forming the biased STEC $\hat{\iota}_{r}^{s}(i)$,

$$\hat{\iota}_{r}^{s}(i)=\iota_{r}^{s}(i)-\frac{1}{\mu_{gf}}d_{gf}^{s} \tag{9}$$

where use has been made of $d_{if}^{s}-d_{,1}^{s}=-\frac{1}{\mu_{gf}}d_{gf}^{s}$; this equality account for the emergence of SDCBs d_{gf}^{s}, which now enter the STEC $\iota_{r}^{s}(i)$.

Next we lump $dt_{r}(i)$ and $d_{r,1}$ into just a single parameter, which reads,

$$\hat{dt}_{r}(i)=dt_{r}(i)+d_{r,1} \tag{10}$$

with $\hat{dt}_{r}(i)$ the biased receiver clocks.

When it comes to the phase observation equations, we have the following equality,

$$d_{if}^{s}+dt_{r}(i)-\iota_{r}^{s}(i)+a_{r,1}^{s}=\hat{dt}_{r}(i)-\hat{\iota}_{r}^{s}(i)+\hat{a}_{r,1}^{s} \tag{11}$$

with $\hat{a}_{r,1}^{s}=a_{r,1}^{s}-d_{r,1}-\frac{1}{\mu_{gf}}d_{gf}^{s}+d_{if}^{s}$ the biased ambiguities.

Considering Equations (9), (10) and (11), we can re-write Equation (8) as

$$\begin{aligned}\hat{p}_{r,1}^{s}(i)&=c_{r}^{s}(i)\cdot\hat{\tau}_{r}(i)+\hat{dt}_{r}(i)+\hat{\iota}_{r}^{s}(i)\\ \hat{\phi}_{r,1}^{s}(i)&=c_{r}^{s}(i)\cdot\hat{\tau}_{r}(i)+\hat{dt}_{r}(i)-\hat{\iota}_{r}^{s}(i)+\hat{a}_{r,1}^{s}\end{aligned} \tag{12}$$

where the $\hat{dt}_{r}(i)$, the $\hat{\iota}_{r}^{s}(i)$ and the $\hat{a}_{r,1}^{s}$ are still not individually estimable, because there is a rank deficiency occurring among them, which is of size one. To solve this we opt for not estimating the biased receiver clocks at the first epoch $\hat{dt}_{r}(1)$, thereby resulting in the full-rank variant of Equation (12), which reads,

$$\begin{aligned}\hat{p}_{r,1}^{s}(i)&=c_{r}^{s}(i)\cdot\hat{\tau}_{r}(i)+\overline{dt}_{r}(i)+\overline{\iota}_{r}^{s}(i)\\ \hat{\phi}_{r,1}^{s}(i)&=c_{r}^{s}(i)\cdot\hat{\tau}_{r}(i)+\overline{dt}_{r}(i)-\overline{\iota}_{r}^{s}(i)+\overline{a}_{r,1}^{s}\end{aligned} \tag{13}$$

where

$$\begin{aligned}\overline{dt}_{r}(i)&=\hat{dt}_{r}(i)-\hat{dt}_{r}(1)=dt_{r}(i)-dt_{r}(1)\\ \overline{\iota}_{r}^{s}(i)&=\hat{\iota}_{r}^{s}(i)+\hat{dt}_{r}(1)=\iota_{r}^{s}(i)-\frac{1}{\mu_{gf}}d_{gf}^{s}+\hat{dt}_{r}(1)\\ \overline{a}_{r,1}^{s}&=\hat{a}_{r,1}^{s}+2\hat{dt}_{r}(1)\end{aligned} \tag{14}$$

with $\overline{dt}_{r}(i)$ the estimable receiver clocks, $\overline{\iota}_{r}^{s}(i)$ the estimable STEC, and $\overline{a}_{r,1}^{s}$ the estimable ambiguities.

Regarding Equation (14), three remarks are in order.

First, the $d\bar{t}_r(i)$ begin to be present at the second epoch and beyond, since they represent the drifts of the original receiver clocks $dt_r(i)$ with respect to the first epoch.

Second, the $\bar{\iota}_r^s(i)$, the ionospheric observables that the PPP technique can estimate from the single-frequency GNSS data, are found to be a linear function of the STEC $\iota_r^s(i)$, the SDCBs d_{gf}^s and the biased receiver clocks at the first epoch $\hat{dt}_r(1)$. Recall the $\tilde{\iota}_r^s(i)$ given in Equation (4), which are the ionospheric observables one can estimate from the dual-frequency GNSS data using the CCL technique. We argue that the $\bar{\iota}_r^s(i)$ are largely similar to the $\tilde{\iota}_r^s(i)$ in terms of interpretation; they both can be used as inputs to the thin-layer ionosphere model (which we shall describe later) for jointly estimating the VTEC parameters and the SDCBs. A closer comparison between the $\bar{\iota}_r^s(i)$ with the $\tilde{\iota}_r^s(i)$ shows that, the $\hat{dt}_r(1)$ can be treated as if they were the $d_{r,gf}$, since they are two nuisance parameters of the same number and nature (receiver-dependent, time-constant). An exception to this arises, however, when a simultaneous loss of lock on all satellites occurs. Starting at the epoch the receiver locks onto a sufficient number of satellites again, the biased receiver clocks at this epoch, instead of $\hat{dt}_r(1)$, begin entering the $\bar{\iota}_r^s(i)$. This means, in this case, that the number of nuisance parameters in the $\bar{\iota}_r^s(i)$ becomes greater than the number of $d_{r,gf}$.

Third, the $\bar{a}_{r,1}^s$ absorb a set of inestimable parameters including $d_{r,1}$, d_{gf}^s, d_{if}^s and $\hat{dt}_r(1)$; this is a direct consequence to rank deficiency elimination. Fortunately, the time constancy of the $\bar{a}_{r,1}^s$ remains unaffected in this process, thereby ensuring the full exploitation of the phase data.

In summary, Equation (13) accounts for the functional model of our PPP technique. For completeness sake, we point out that we base the stochastic modeling of the GNSS observables on the elevation-dependent weighting strategy. Moreover, in addition to precise satellite orbit and clock products, we also consider applying a

number of corrections, including the solid Earth tide, the phase wind-up effects, and the satellite and receiver phase center offsets and variations, to the code and phase data.

Thin-layer ionosphere model

As we mentioned earlier, one needs to refer to the thin-layer ionosphere model to estimate the VTEC, along with the SDCBs, from the ionospheric observables whose inverse covariance matrix is used as weight matrix. Roughly speaking, this model takes advantage of two facts. First, the STEC can vary, and this variability is driven by a variety of factors of which geomagnetic latitude, local time and elevation angle are most prominent. Second, the SDCBs and other nuisance parameters, such as the RDCBs, likely remain constant over time under normal environmental conditions.

The thin-layer model exploits the first fact by approximating the whole ionosphere with a spherical shell located at a pre-specified height, say, 450 kilometers, above the Earth's surface. At the points where satellite-to-receiver ray paths pierce the shell, called the Ionospheric Penetration Points (IPPs), we relate the STEC $\iota_r^s(i)$ and the VTEC $v_r^s(i)$ using a mapping function $M_r^s(i)$ which reads (Brunini and Azpilicueta 2009),

$$\frac{1}{M_r^s(i)} = \sqrt{1-\left(\frac{R}{R+450}\right)^2 \cdot \cos^2\left[e_r^s(i)\right]} \tag{15}$$

with $\iota_r^s(i) = M_r^s(i) \cdot v_r^s(i)$ and where R is the mean Earth's radius in kilometer, and $e_r^s(i)$ is the elevation angle of satellite s as seen from receiver r at epoch i.

Next, this model mathematically characterizes the temporal and spatial variability of the $v_r^s(i)$ as, for instance, the sum of a polynomial function and a finite Fourier series (Li et al. 2015),

$$v_r^s(i) = \sum_{a=0}^{2}\sum_{b=0}^{2}\left\{E_{ab}\left(\Psi_{IPP}-\Psi_{REC}\right)^a \Lambda_{IPP}^b\right\} + \sum_{k=1}^{4}\left\{C_k \cos\left(k\Lambda_{IPP}\right) + S_k \sin\left(k\Lambda_{IPP}\right)\right\} \tag{16}$$

where Ψ_{IPP} and Ψ_{REC} denote, respectively, the geomagnetic latitudes of the IPPs

and of the receivers. $\Lambda_{IPP} = \frac{2\pi(t_i - 14)}{24}$ denotes the solar longitudes of the IPPs, with t_i the local time to which the epoch i corresponds. E_{ab}, C_k and S_k are coefficients that are unknown.

We conclude this section with Figure 1, which depicts the schematic diagram of DF approach, and that of our SF approach. By the use of this figure we review the primary features of each approach as follows.

The DF approach adopts GNSS data at two distinct frequencies, and it consists of two sequential steps. In the first step, we construct the geometry-free code and phase observables, to which, we apply the CCL technique in order to obtain the ionospheric observables, interpreted as a linear combination of the STEC, the SDCBs and the RDCBs. The thin-layer ionosphere model fulfills the role of isolating the interested parameters (the VTEC and the SDCBs), along with the nuisance ones (the RDCBs), from the ionospheric observables.

Our SF approach is fairly similar in implementation to the DF approach, but it bases joint estimation of the VTEC parameters and the SDCBs merely on single-frequency GNSS code and phase data corrected by the precise satellite orbit and clock products externally provided by, for instance, the IGS. The task of retrieving the ionospheric observables, containing the STEC, the SDCBs and the biased receiver clocks at the first epoch, is now accomplished by the PPP technique. After this, we again turn to the thin-layer ionosphere model.

3. Results

We begin this section by describing the experimental setup, followed by illustrating numerical results, from which the major findings we identify are also detailed.

Experimental Setup

We applied the DF as well as our SF approaches to two sets of GPS data, collected by receivers of different types (mass-market, geodetic-grade) under different ionospheric conditions (solar activity, geomagnetic latitude). This is helpful for us to gain a thorough understanding of the overall performance of each approach.

The first set of GPS data was sampled every 30 seconds by four co-located receivers during April 19 (DOY 110) to May 25 (DOY 146), 2016. These receivers, designated respectively as CUAU, SPU3, CUT2 and SPA8, are deployed at the main campus of Curtin University (Perth, Australia), and the distance between any two of them does not exceed 400 meters. We point out further that, CUAU and SPU3 are two low-cost UBLOX EVK-M8T receivers, connected to geodetic-grade antennas and offering GPS L1 data. Would one use patch antennas, the data so collected can be prone to severe multipath effects. One solution to this issue is to use the modified sidereal filtering (Choi et al. 2004), but we leave this outside the scope of our current analysis. The CUT2 and SPA8 are, respectively, a TRIMBLE NETR9 receiver and a SEPTENTRIO POLARXS receiver; they supply GPS L1+L2 data for our use. In addition, because of the co-location, the effects due to the ionosphere on GPS data ought to be same for each receiver. We shall draw on this fact in the following analysis.

The second set of GPS L1+L2 data was collected by a few hundreds of globally distributed receivers (see Figure 2 for their locations) at a 30-second sampling rate, during a solar maximum month March 2014 and a solar minimum month March 2015, namely, two separate months one year apart.

On a receiver-by-receiver and day-by-day basis, we generated one or two daily time series of the VTEC for the IPPs at the zenith of each GPS receiver, called zenith VTEC; each time series represents results obtained from a particular approach. Note that this process also produced the daily estimates of the SDCBs for GPS satellites in view of each receiver.

In our data processing, we used a cut-off elevation angle of 30 degrees so as to discard particularly noisy GPS data. We empirically set the zenith-referenced standard deviation to 30 cm for the code and to 0.3 cm for the phase. When implementing the PPP, a least-square batch adjustment is used to process the GPS L1 data, corrected by IGS Final orbit and clock products, into ionospheric observables along with their covariance matrix. We estimated the ZTDs as piece-wise constants with an update rate of two hours. In addition, we aligned the C1, if any, to the P1 using the monthly values of P1-C1 SDCBs published by the Center for Orbit Determination in Europe (CODE). This implies that, the type of the SDCBs that two

approaches deliver is always P1-P2.

Results of the first data set

We focus first on Figure 3, depicting the ionospheric observables determined for two receivers SPU3 and SPA8 from their GPS L1 (using the PPP) or L1+L2 (using the CCL) data collected on May 5, 2016 (which is an arbitrary choice). We split this figure into three panels for clearer presentation, with each panel showing the results for a different receiver or data source. Moreover, in each panel the results for different GPS satellites are colored differently. Taken together, we make three remarks here. First, we see that in this case the ionospheric observables can take negative values for some satellites, for instance PRN 23, as marked with an arrow. This is, however, not unexpected, given their interpretation (see Equations 4 and 14). Second, considering, again, the ionospheric observables obtained for GPS satellite 23 in Figures 3a-3c, they follow an order of increasing smoothness, thereby indicating that their quality is mainly driven by the code data. Third, as should be the case, we can readily recognize that the overall pattern in the ionospheric observables is more or less identical from panel to panel, with higher spatio-temporal variability and larger magnitudes at daytime than at night, reflecting the typical signature of the ionosphere.

Now turn to Figure 4, where each panel shows five time series of zenith VTEC estimates with a time resolution of five minutes for a pair of mixed receivers (one low-cost UBLOX receiver and one geodetic-grade receiver), and for one randomly selected day. Overall, it follows that in each panel the three time series, shown with solid lines and referred to the left y axis, agree well with one another; in accordance with our expectation, each time series exhibits a pronounced diurnal variation, with maxima and minima near local noon and midnight, respectively. To further quantify this agreement, we calculated the mean bias and the standard deviation (STD) for two SF time series (solid red and green lines) by using the corresponding DF time series (solid blue line) as a reference, and present the results in Table 1. Note further that in each panel the dashed red and green lines with asterisks (referred to the right y axis) show, respectively, the two SF time series that each has been differenced with respect to the DF time series. The main conclusion to be drawn from Figure 4, in conjunction with Table 1, is straightforward. The application of our

SF approach to GPS L1 data provided by a geodetic-grade receiver (SPA8 or CUT2) and by a low-cost receiver (SPU3 or CUAU) shall deliver VTEC estimates of virtually the same quality, as evidenced by the fact that these estimates have approximately the same mean biases and STD values (see Table 1). This appears to be quite favorable, since it justifies the subsequent analysis of our SF approach using a global network of geodetic-grade receivers (instead of low-cost ones, which are not available), from which further findings we shall draw can still be considered representative.

It is noteworthy that, along with the zenith VTEC estimates discussed above, we obtained also daily estimates of SDCBs, whose offsets with respect to the corresponding monthly products delivered by the CODE, expressed in absolute values (and thus called absolute offsets hereafter), are shown in Figure 5, following the same arrangement as Figure 4. Let us refer to the percentage of satellites with absolute offsets less than 1 nanosecond as a performance measure. Then it follows that, such a percentage for the DF approach resides between 78% (Figure 5f) and 97% (Figure 5c), generally lower than that for our SF approach, amounting to 100% for red bars and varying from 90% (Figure 5d) to 100% (Figures 5a and 5f) for green bars. This implies that DF approach can perform worse than our SF approach, as far as the single-receiver based SDCB estimation is concerned. We surmise this may be attributed to two reasons. First, whereas the CCL assumes the geometric effects on GPS data to be completely unknown, the PPP exploits a-priori knowledge about the geometric effects by taking advantage of precise satellite orbit and clock products externally provided as corrections. Second, more importantly, the DF approach is susceptible to the systematic errors induced by time-varying RDCBs (Ciraolo et al. 2007). Roughly speaking, one assumption, tacitly made by the DF approach, that RDCBs remain constant over time, is in very many cases definitely contradictory to the experimental facts. Fortunately, this is not the case with our SF approach, since the ionospheric observables from which it estimates the SDCBs are RDCB-free.

Results of the second data set

The experimental results so far reported are not altogether adequate, since they were obtained under limited ionospheric conditions (37 consecutive days, four

receivers at a middle-latitude site), and thus lead to findings which, though suggestive, are by no means conclusive. For this reason, we further processed the second set of GPS data, in order to ascertain how well our SF approach works under diverse ionospheric conditions. Considering the fact that we have got a large set of results, we do not attempt to cover all of them; rather, without loss of generality and for the sake of clarity, we shall only present the results for 12 receivers whose geographic locations are highlighted in Figure 2 with black stars.

Let us focus first on Figure 6, consisting of six panels, with each showing two time series of zenith VTEC estimates determined using, respectively, L1+L2 and L1 data from a common receiver with a time resolution of five minutes. Each time series covers a period of 24 hours from 12:00 am to 12:00 am (UTC) next day, or more precisely, one full day in March 2014, a solar maximum month. It is worth mentioning that, six receivers involved here are divisible into three pairs, with each pair being located in in high-, middle- and low-latitude regions, respectively. See the leftmost four columns of Table 2 (top block) for more details. Using the DF time series (blue line) as a reference, we calculated, on a panel-by-panel basis, two quality measures including the mean bias and the STD, for the SF time series (red line), and present the results in the last column of Table 2 (top block). Two findings emerge here. First, our SF approach is capable to deliver zenith VTEC estimates that are close to unbiased, as evidenced by the fact that, the mean biases computed are small in magnitude and can be considered insignificant from a practical viewpoint. Second, the quality of SF time series decreases as the level of the ionospheric activity increases. Notably, the high STD values (between 1.60 and 1.75 TECU) occur at two low-latitude sites, IQQE and ADIS, which are near the geomagnetic equator and most likely subject to disturbed ionospheric activity. As compared to this worst-case scenario, we see reduced STD values for the remaining four sites by a factor of more than two owing to relatively calm ionospheric activity.

Figure 7 is analogous to Figure 6, except that it involves different receivers and different days in March 2015, a solar minimum month. Likewise, Table 2 (bottom block) summarizes the receiver characteristics and the statistics of the SF time series. The present results not only confirm the two findings above, but also reveal that the SF time series obtained for a middle-latitude site DUND at day 60 of 2015 exhibits

the lowest mean bias (-0.07 TECU) and also the smallest STD (0.38 TECU), thus corresponding to a best-case scenario. We attribute this superior performance to the fact that the thin-layer ionosphere model is highly likely to work well under calm ionospheric conditions.

Finally, we direct our attention to the daily estimates of SDCBs, which we obtain together with the daily time series of zenith VTEC estimates shown in Figures 6 and 7. For conciseness, we shall restrict ourselves to the results (given in Figure 8 as absolute offsets) for six (instead of 12) receivers and for six (instead of nine) days. Consider, again, the percentage of satellites with absolute offsets less than 1 nanosecond as a performance measure. We see, for our SF approach, that, this percentage is as high as 96% (Figures 8d-8f) at the solar minimum month (March 2015), irrespective of the locations of the receivers; this value drops and can vary from 73% (Figure 8c) to 85% (Figure 8a) at the solar maximum month (March 2014). Under these scenarios, both DF and our SF approaches perform close to each other. However, an obvious exception occurs for a low-latitude site (ADIS) and for a day in March 2014 (DOY 60), where the percentage experienced by DF approach is 36%.

4. Conclusions

The customary dual-frequency (DF) approach for joint estimation of Vertical Total Electron Content (VTEC) and Satellite Differential Code Biases (SDCBs) requires GNSS code and phase data on two frequencies, and can be characterized by two sequential steps: retrieving ionospheric observables and applying to them a thin-layer ionospheric model.

In this work, we have developed a single-frequency (SF) approach, which retains exactly the same applicability as the DF approach, but, in addition to this, has the marked advantage of being workable with low-cost mass-market GNSS receivers, providing code and phase data on only one frequency. Both DF and our SF approaches follow the same two-step process; the main difference lies in that, they employ, respectively, the Carrier-to-Code Leveling (CCL) and the Precise Point Positioning (PPP) to implement the first step.

We assessed the performance of our SF approach on two sets of GPS real data. The first data set, covering a time period of 37 consecutive days, was collected by

two mass-market and two geodetic-grade receivers that were deployed close to each other at a middle-latitude site. The second data set came from a global network of approximately 200 geodetic-grade receivers for the solar minimum month March 2014 and the solar maximum month March 2015. On a receiver-by-receiver, day-by-day basis, use has been made of DF and/or our SF approaches to estimate daily time series of zenith VTEC with a time resolution of five minutes, along with daily estimates of SDCBs for GPS satellites in view of each receiver. Empirical analysis of the results so obtained warrants two conclusions.

First, both approaches are capable of delivering zenith VTEC estimates that are reasonably consistent. For a common receiver (or multiple co-located receivers), the overall consistency between two daily time series derived, respectively, by DF and our SF approaches, in terms of STD, is found to be at the level of a few tenths of a TECU to roughly 2 TECU.

Second, our SF approach appears promising as a means to calibrate SDCBs under varying ionospheric conditions; it can provide daily estimates of SDCBs with absolute offsets less than 1 nanosecond for 73 to 96 percent of GPS satellites in view, considering as a reference the monthly products published by the CODE. When it comes to the DF approach, this percentage stays more or less the same in most cases, but may drop sharply to less than 40% during extremely disturbed ionospheric conditions.

Acknowledgements

This work was partially funded by the National key Research Program of China "Collaborative Precision Positioning Project" (No. 2016YFB0501900) and the National Natural Science Foundation of China (Nos. 41604031, 41774042). The first author is supported by the CAS Pioneer Hundred Talents Program. All this support is gratefully acknowledged.

References

Artru J, Ducic V, Kanamori H, Lognonné P, Murakami M (2005) Ionospheric detection of gravity waves induced by tsunamis. Geophysical Journal International 160:840-848

Banville S, Collins P, Zhang W, Langley RB (2014) Global and regional ionospheric corrections for faster PPP convergence. Navigation 61:115-124

Brunini C, Azpilicueta F (2010) GPS slant total electron content accuracy using the single layer model under different geomagnetic regions and ionospheric conditions. J Geodesy 84:293-304

Brunini C, Azpilicueta FJ (2009) Accuracy assessment of the GPS-based slant total electron content. J Geodesy 83:773-785

Brunini C, Camilion E, Azpilicueta F (2011) Simulation study of the influence of the ionospheric layer height in the thin layer ionospheric model. J Geodesy 85:637

Brunini C, Meza A, Gende M, Azpilicueta F (2008) South American regional ionospheric maps computed by GESA: A pilot service in the framework of SIRGAS. Advances in Space Research 42:737-744

Choi K, Bilich A, Larson KM, Axelrad P (2004) Modified sidereal filtering: implications for high-rate GPS positioning. Geophysical research letters, 2004, 31(22).

Choi KH, Lee JY, Kim HS, Kim J, Lee HK (2012) Simultaneous estimation of ionospheric delays and receiver differential code bias by a single GPS station. Measurement Science and Technology 23:065002

Ciraolo L, Azpilicueta F, Brunini C, Meza A, Radicella S (2007) Calibration errors on experimental slant total electron content (TEC) determined with GPS. J Geodesy 81:111-120

Cohen CE, Penm B, Parkinson BW Estimation of absolute ionospheric delay exclusively through single-frequency GPS measurements. In: Proceedings of the 5th International Technical Meeting of the Satellite Division of The Institute of Navigation (ION GPS 1992), 1992. pp 325-330

Dautermann T, Calais E, Haase J, Garrison J (2007) Investigation of ionospheric electron content variations before earthquakes in southern California, 2003–2004. Journal of Geophysical Research: Solid Earth 112

Dettmering D, Limberger M, Schmidt M (2014) Using DORIS measurements for modeling the vertical total electron content of the Earth's ionosphere. J Geodesy 88:1131-1143

Dyrud L, Jovancevic A, Brown A, Wilson D, Ganguly S (2008) Ionospheric measurement with GPS: Receiver techniques and methods. Radio Science 43

Feltens J (2003) The international GPS service (IGS) ionosphere working group. Advances in Space Research 31:635-644

Gulyaeva TL, Arikan F, Hernandez-Pajares M, Veselovsky I (2014) North-south components of the annual asymmetry in the ionosphere. Radio Science 49:485-496

Hernández-Pajares M, Juan J, Sanz J (1999) New approaches in global ionospheric determination using ground GPS data. Journal of Atmospheric and Solar-Terrestrial Physics 61:1237-1247

Hernández-Pajares M, Juan JM, Sanz J, Orus R, Garcia-Rigo A, Feltens J, Komjathy A, Schaer SC, Krankowski A (2009) The IGS VTEC maps: a reliable source of ionospheric information since 1998. J Geodesy 83:263-275

Komjathy A et al. (2012) Detecting ionospheric TEC perturbations caused by natural hazards using a global network of GPS receivers: The Tohoku case study. Earth, planets and space 64:1287-1294

Komjathy A, Sparks L, Wilson BD, Mannucci AJ (2005) Automated daily processing of more than 1000 ground-based GPS receivers for studying intense ionospheric storms. Radio Science 40

Kouba J, Héroux P (2001) Precise point positioning using IGS orbit and clock products. GPS solutions 5:12-28

Leick A, Rapoport L, Tatarnikov D (2015) GPS satellite surveying. John Wiley & Sons,

Li Z, Yuan Y, Wang N, Hernandez-Pajares M, Huo X (2015) SHPTS: towards a new method for generating precise global ionospheric TEC map based on spherical harmonic and generalized trigonometric series functions. J Geodesy 89:331-345

Liu Z, Gao Y (2004) Ionospheric TEC predictions over a local area GPS reference network. GPS Solutions 8:23-29

Lognonné P et al. (2006) Ground-based GPS imaging of ionospheric post-seismic signal. Planetary and Space Science 54:528-540

Mannucci A, Wilson B, Yuan D, Ho C, Lindqwister U, Runge T (1998) A global mapping technique for GPS-derived ionospheric total electron content measurements. Radio science 33:565-582

Mannucci AJ, Wilson BD, Edwards CD (1993) A new method for monitoring the Earth's ionospheric total electron content using the GPS global network. In: Proceedings of ION GPS-93, the 6th international technical meeting of the satellite division of The Institute of Navigation, Salt Lake City, UT, 22–24 September 1993, pp 1323–1332

Montenbruck O, Hauschild A, Steigenberger P (2014) Differential Code Bias Estimation using Multi-GNSS Observations and Global Ionosphere Maps. Navigation 61:191-201

Park J, von Frese RR, Grejner-Brzezinska DA, Morton Y, Gaya-Pique LR (2011) Ionospheric detection of the 25 May 2009 North Korean underground nuclear test. Geophys Res Lett 38

Sardon E, Rius A, Zarraoa N (1994a) Estimation of the transmitter and receiver differential biases and the ionospheric total electron content from Global Positioning System observations. Radio Science 29:577-586

Sardon E, Rius A, Zarraoa N (1994b) Ionospheric calibration of single frequency VLBI and GPS observations using dual GPS data. J Geodesy 68:230-235

Schüler T, Oladipo OA (2013) Single-frequency GNSS retrieval of vertical total electron content (VTEC) with GPS L1 and Galileo E5 measurements. Journal of Space Weather and Space Climate 3:A11

Schüler T, Oladipo OA (2014) Single-frequency single-site VTEC retrieval using the NeQuick2 ray tracer for obliquity factor determination. GPS solutions 18:115-122

Sezen U, Arikan F, Arikan O, Ugurlu O, Sadeghimorad A (2013) Online, automatic, near-real time estimation of GPS-TEC: IONOLAB-TEC. Space Weather

11:297-305

Stephens P, Komjathy A, Wilson B, Mannucci A (2011) New leveling and bias estimation algorithms for processing COSMIC/FORMOSAT-3 data for slant total electron content measurements. Radio Science 46

Wang N, Yuan Y, Li Z, Montenbruck O, Tan B (2016) Determination of differential code biases with multi-GNSS observations. J Geodesy 90:209-228

Xia R Determination of absolute ionospheric error using a single frequency GPS receiver. In: Proceedings of the 5th International Technical Meeting of the Satellite Division of The Institute of Navigation (ION GPS 1992), 1992. pp 483-490

Yao Y, Chen P, Zhang S, Chen J (2013) A new ionospheric tomography model combining pixel-based and function-based models. Advances in Space Research 52:614-621

Zumberge J, Heflin M, Jefferson D, Watkins M, Webb FH (1997) Precise point positioning for the efficient and robust analysis of GPS data from large networks. Journal of Geophysical Research: Solid Earth 102:5005-5017

Table 1. Descriptive statistics for two daily time series of zenith VTEC estimates derived using GPS L1 data (dashed red and green lines with asterisks in Figure 4): mean bias | standard deviation (STD), in TECU.

DOY	SF & SPA8	SF & SPU3	SF & CUT2	SF &CUAU
110	-0.07|0.30	0.33|0.33	n/a	n/a
126	-0.07|0.42	0.34|0.41	n/a	n/a
140	0.18|0.19	0.46|0.21	n/a	n/a
111	n/a	n/a	0.39|0.61	0.13|0.57
139	n/a	n/a	-0.44|0.63	-0.30|0.47
141	n/a	n/a	0.47|0.42	0.71|0.37

Table 2. The main characteristics of 12 receivers involved in Figures 6 and 7, as well as the mean bias and the standard deviation (STD) (both expressed in in TECU) of the SF time series (red line), computed using the corresponding DF time series (blue line) as a reference.

Station	DOY	Receiver type	Longitude-latitude	Mean bias | STD
BAKE	73	TPS NET-G3A	96.0° W, 64.3° N	0.28|0.68
NRC1	61	JAVAD TRE_G3TH DELTA	75.6° W, 45.5° N	-0.35|0.64
ADIS	60	JPS LEGACY	38.8° E, 9.0° N	-0.28|1.75
OHI3	88	LEICA GR25	57.9° W, 63.3° S	0.23|0.55
SUTV	60	JPS EGGDT	20.8° E, 32.4° S	0.21|0.77
IQQE	79	TRIMBLE NETR9	70.1° W, 20.3° S	-0.32|1.60
SVTL	74	JAVAD TRE_G3TH DELTA	29.8° E, 60.5° N	-0.28|0.53
LAMA	80	LEICA GRX1200+GNSS	20.7° E, 53.8° N	-0.14|0.58
DAKR	71	TPS NET-G3A	17.4° W, 14.7° N	-0.24|0.94
MAW1	78	LEICA GRX1200GGPRO	62.9° E, 67.6° S	0.16|0.44
DUND	80	TRIMBLE NETR9	170.6° E, 45.9° S	-0.07|0.38
ULDI	79	TRIMBLE NETRS	31.4° E, 28.3° S	-0.36|0.90

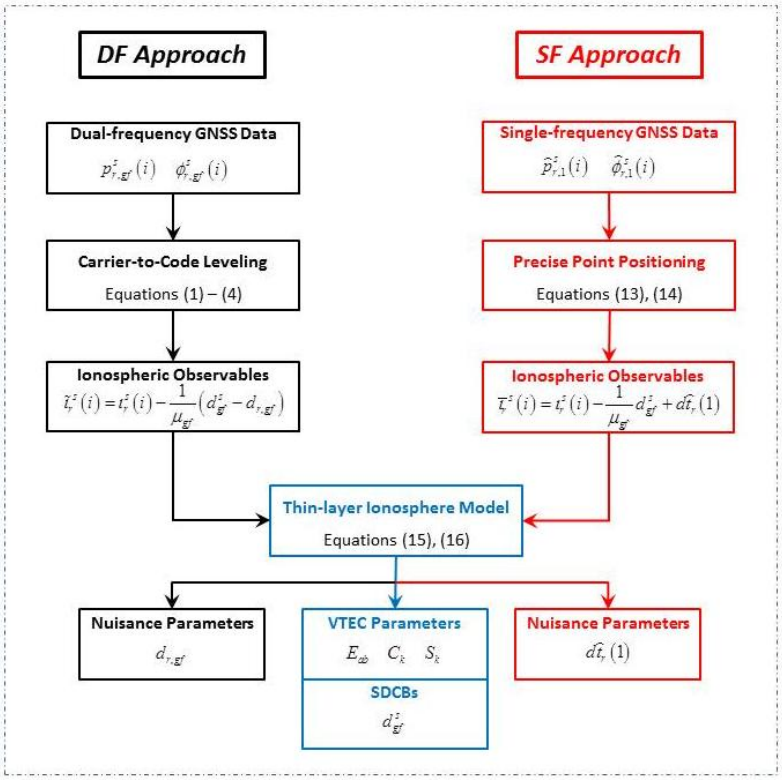

Figure 1. Schematic diagram of the customary DF approach (in black), and that of our SF approach (in red); the middle part shown in blue is common to both approaches.

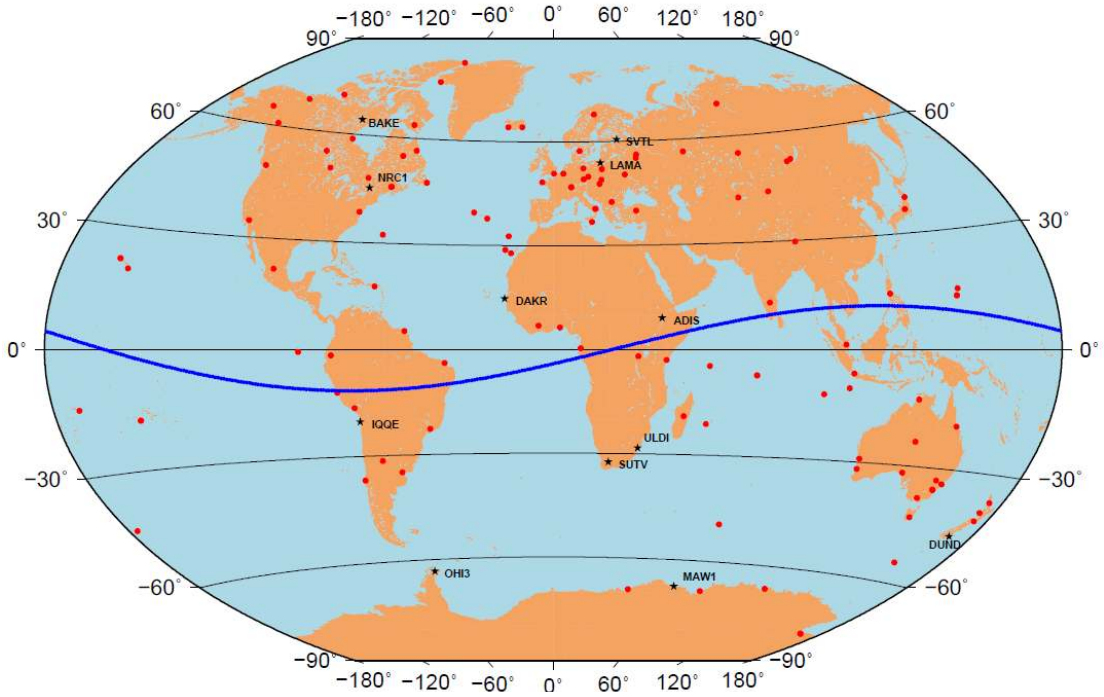

Figure 2. Geographic locations of a few hundreds of receivers (solid red dots) that provide the second set of GPS data analyzed in this work. The blue line marks the geomagnetic equator. The black stars highlight 12 receivers, deployed in the high-, middle- and low-latitude regions.

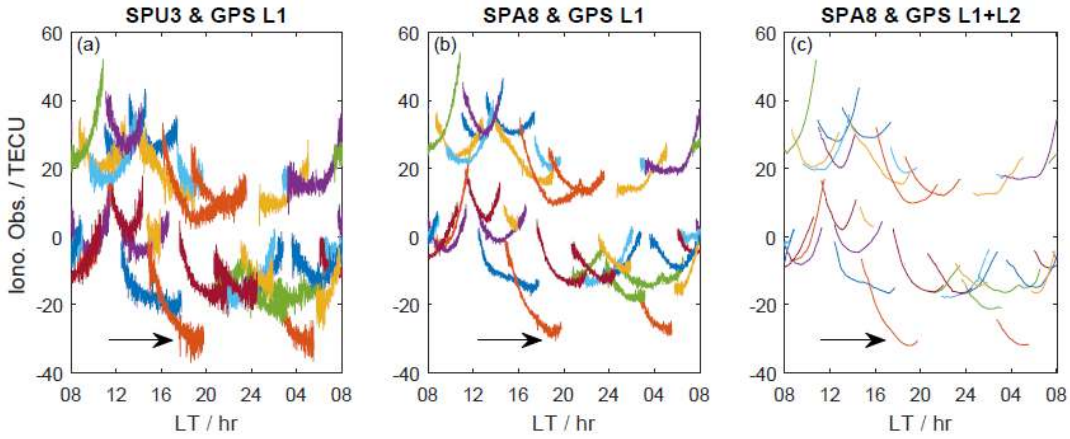

Figure 3. Ionospheric observables (in TECU) extracted from GPS L1 or L1+L2 data for receivers SPU3 and SPA8 on May 5 (DOY 126), 2016, and shown as a function of Local Time (UTC+8). Different colors correspond to different satellites. In each panel, the arrow points to the results for GPS satellite 23.

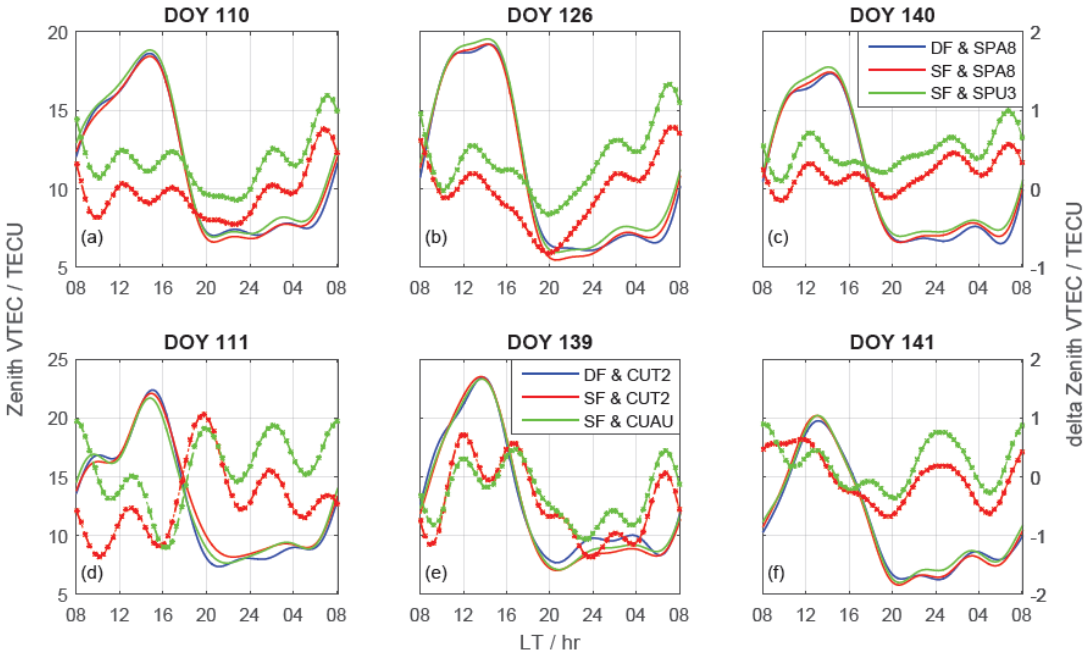

Figure 4. Time series of zenith VTEC estimates with a 5-min time resolution for a single experimental day that is randomly selected. We arrange a total of six panels in two rows, with each row representing the results for one pair of mixed receivers (one mass-market and one geodetic-grade). Each panel contains five lines. The solid blue and red lines (referred to the left y axis) represent two daily time series obtained using, respectively, L1+L2 and L1 GPS data from a geodetic-grade receiver (SPA8 or CUT2); the green line (referred to the left y axis) represents the time series obtained using L1 data from a low-cost receiver (SPU3 or CUAU). The dashed red and green lines with asterisks (referred to the right y axis) show, respectively, the two SF time series (solid red and green lines) that each has been differenced with respect to the corresponding DF time series (solid blue line).

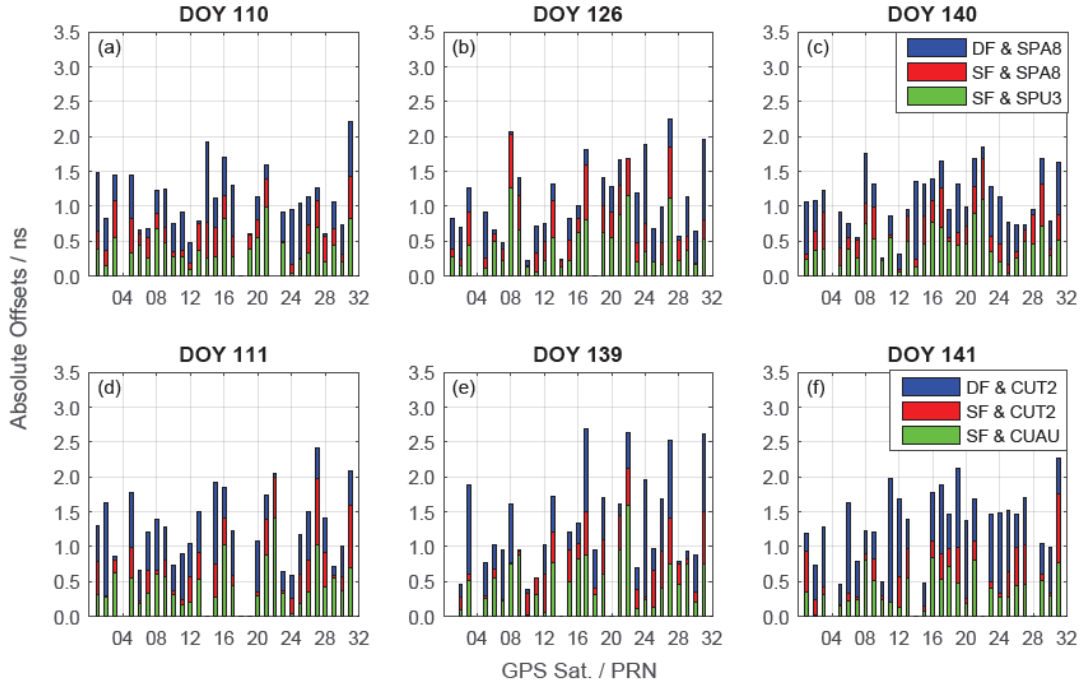

Figure 5. Absolute offsets between the daily estimates of SDCBs, obtained along with daily time series of zenith VTEC estimates depicted in Figure 4, and the corresponding monthly products published by the Center for Orbit Determination in Europe (CODE). The arrangement of this figure is the same as that of Figure 4. In all panels, the results for each GPS satellite are shown by stacking the three bars on top of each other.

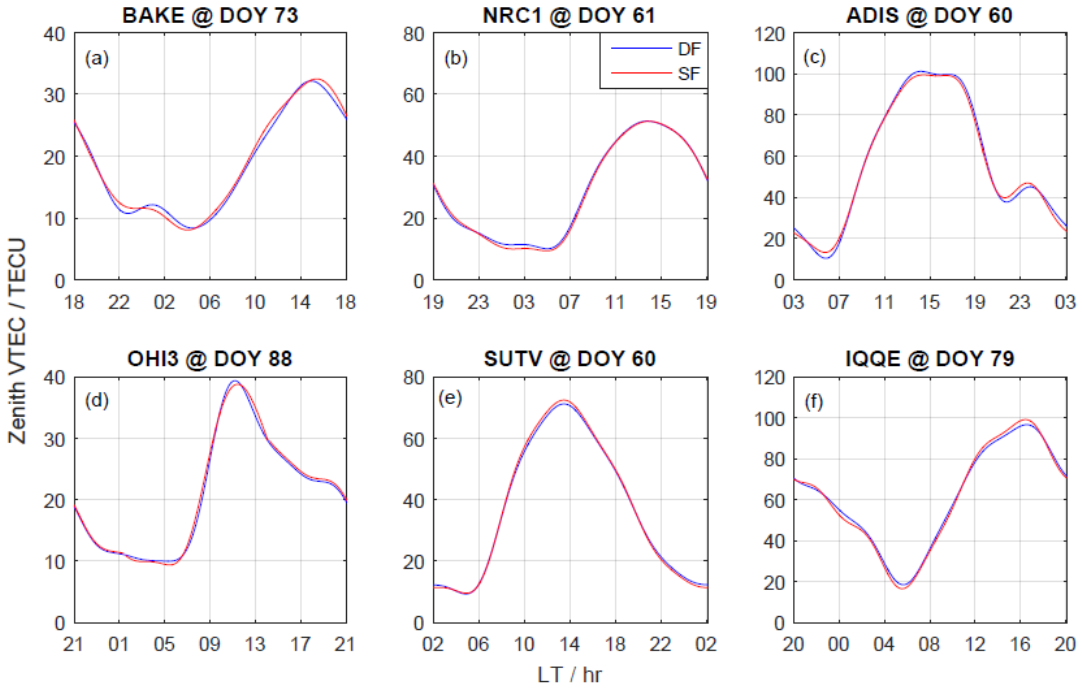

Figure 6. Two daily time series of zenith VTEC estimates with a 5-min time resolution, estimated, respectively, from GPS L1+L2 data (in blue) and from GPS L1 data (in red) collected by a common receiver on a day in March 2014. Six panels, arranged in three columns, show the results for three pairs of receivers, which, from left to right, are located in high-, middle- and low-latitude regions.

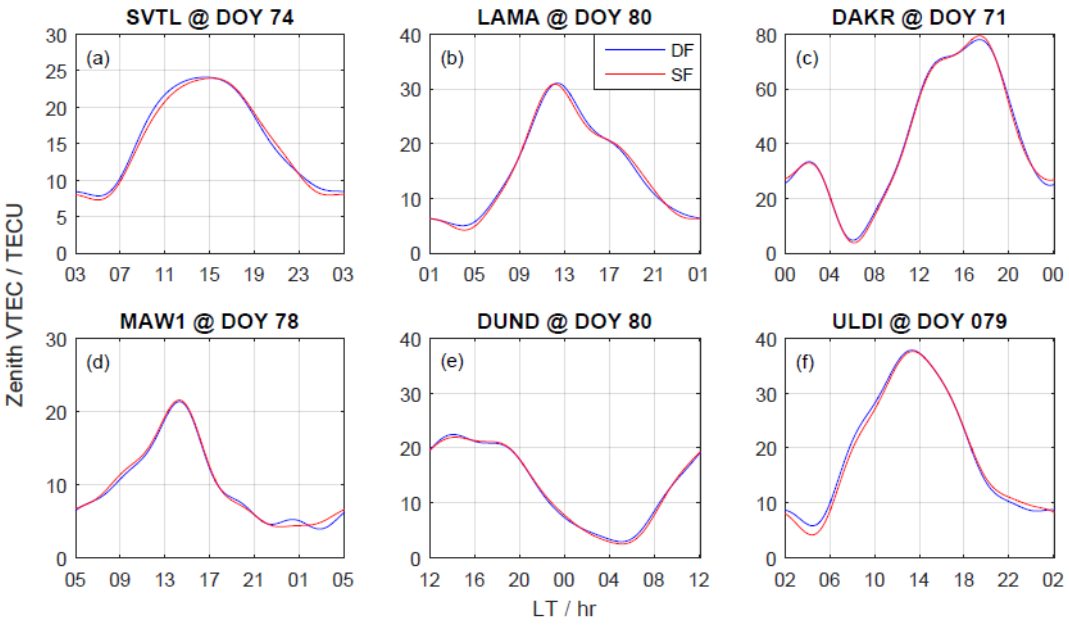

Figure 7. Panels (a)-(f) are analogous to those in Figure 6, except that they show results for another six receivers spread throughout the globe and for a few days in March 2015.

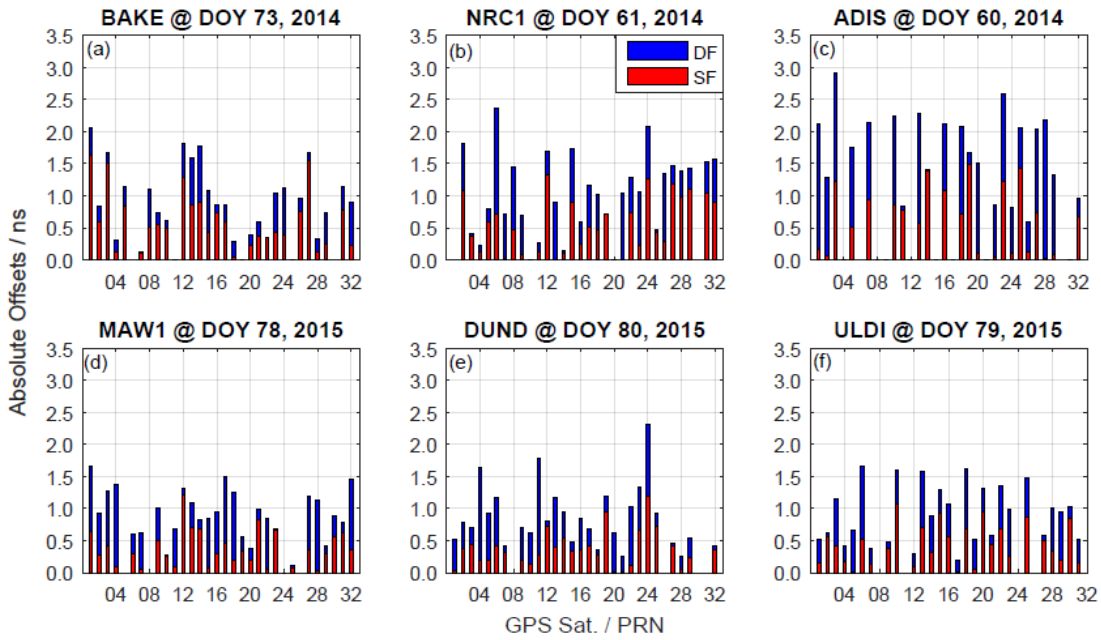

Figure 8. Panels (a)-(f): daily estimates of SDCBs, obtained along with daily time series of zenith VTEC estimates depicted in Figures 6a, 6b, 6c, 7d, 7e and 7f. In each panel, the results are given as absolute offsets in nanosecond relative to the corresponding monthly products published by the Center for Orbit Determination in Europe (CODE).